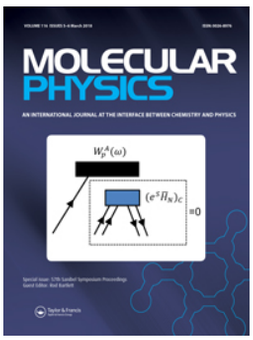

Taylor & Francis
Taylor & Francis Group

Molecular Physics

An International Journal at the Interface Between Chemistry and Physics

ISSN: 0026-8976 (Print) 1362-3028 (Online) Journal homepage: https://www.tandfonline.com/loi/tmph20

Study of the In_2O_3 molecule in the free state and in the crystal

Ilya G. Kaplan, Ulises Miranda & Leonid I. Trakhtenberg

To cite this article: Ilya G. Kaplan, Ulises Miranda & Leonid I. Trakhtenberg (2018) Study of the In_2O_3 molecule in the free state and in the crystal, Molecular Physics, 116:5-6, 678-685, DOI: 10.1080/00268976.2017.1414963

To link to this article: https://doi.org/10.1080/00268976.2017.1414963

MOLECULAR PHYSICS, 2018
VOL. 116, NOS. 5–6, 678–685
https://doi.org/10.1080/00268976.2017.1414963

Taylor & Francis
Taylor & Francis Group

57TH SANIBEL SYMPOSIUM

Study of the In_2O_3 molecule in the free state and in the crystal

Ilya G. Kaplan[a], Ulises Miranda [b] and Leonid I. Trakhtenberg[b,c]

[a]Instituto de Investigaciones en Materiales , Universidad Nacional Autónoma de México, Ciudad de México , Mexico; [b]Department of Kinetics and Catalysis, Semenov Institute of Chemical Physics Russian Academy of Sciences, Moscow, Russia; [c]SSC RF 'Karpov Institute of Physical Chemistry', Moscow, Russia

ABSTRACT

The nanomaterials based on the In_2O_3 molecule are widely used as catalysts and sensors among other applications. In the present study, we discuss the possibility of using nanoclusters of In_2O_3 as molecular photomotors. A comparative analysis of the electronic structure of the In_2O_3 molecule in the free state and in the crystal is performed. For the free In_2O_3 molecule the geometry of its lowest structures, V-shape and linear, was optimised at the CCSD(T) level, which is the most precise computational method applied up to date to study In_2O_3. Using experimental crystallographic data, we determined the geometry of In_2O_3 in the crystal. It has a zigzag, not symmetric structure and possesses a dipole moment with magnitude slightly smaller than that of the V-structure of the free molecule (the linear structure due to its symmetry has no dipole moment). According to the Natural Atomic population analysis, the chemical structure of the linear In_2O_3 can be represented as O = In−O−In = O; the V-shaped molecule has the similar double- and single-bond structure. The construction of nanoclusters from 'bricks' of In_2O_3 with geometry extracted from crystal (or nanoclusters extracted directly from crystal) and their use as photo-driven molecular motors are discussed.

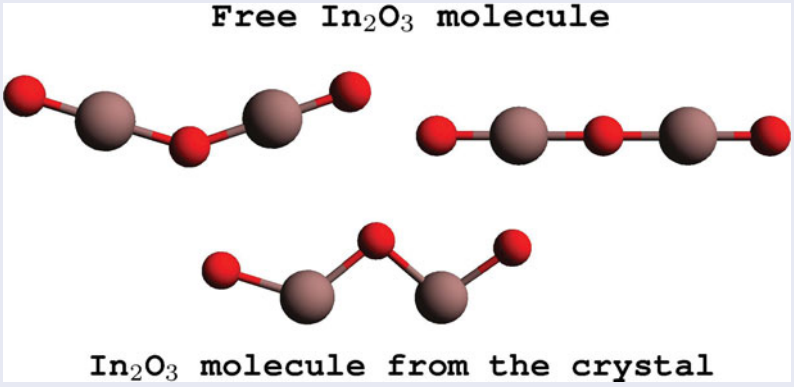

ARTICLE HISTORY
Received 13 April 2017
Accepted 27 November 2017

KEYWORDS
In_2O_3; molecular motors; crystal structure; dipole moment; nature of bonding

1. Introduction

Currently, metallic oxides are considered as promising materials, which are widely used in various fields of application. Among these oxides, In_2O_3 occupies a special place. This semiconductor has a fairly narrow forbidden zone and very shallow electron traps. Consequently, the conduction band is quite rich in electrons even at relatively low temperatures. Indium oxide belongs to the so-called transparent conducting oxides (TCOs) and for nearly 50 years has been one of the dominant TCOs. This material has had applications as catalysts [1–3] and as sensors [4–7], among others. The nanoclusters from the In_2O_3 molecules are also interesting as molecular motors, in particular photo-driven molecular motors, or photomotors, see for example, Refs. [8–10]. As will be shown in this paper, nanoclusters containing In_2O_3 molecules can have permanent as well as induced essential dipole moments, which are very important for different types of molecular motors, see discussion in Subsection 3.3. However, before considering nanoclusters it is important to clarify the structure of the 'bricks', that is, the In_2O_3 molecules, from which these clusters are formed.

Since the production of single crystals of In_2O_3 [11] and the refinement of their structure by means of X-ray diffraction data [12] two years later, many experimental and theoretical studies [13–15] have been developed in order to understand this system. Nevertheless, there

CONTACT Ulises Miranda mirandaulises@yandex.ru

is very limited and somewhat ambiguous information concerning the electronic structure or other data of the free molecule of the sesquioxide. We also point that, to the best of our knowledge, only one experimental study [16] of this molecule is available. Below we present a short account of the research performed on the free In_2O_3 molecule and its clusters.

In 1992, Burkholder *et al.* [16] conducted matrix infrared spectroscopy studies of matrix-isolated gallium and indium oxides in argon matrices. The authors observed a broad band at 826 cm^{-1} and assigned it to the linear In_2O_3, in analogy with Al_2O_3. Four years later, Archibong and Sullivan [17] performed geometry optimisations of M_2O_3 oxides (M = Ga, In and Tl) using Møller–Plesset perturbation theory (MP2), quadratic configuration interaction (QCISD(T)) and density-functional theory (DFT-B3LYP) methods. Starting from V-shaped geometries, their MP2 optimisations ended with the linear structure. It had the lowest energy and the vibrational frequency of the most intense stretching band, 888 cm^{-1} scaled by 0.93 [17], was equal to the experimental value, 826 cm^{-1} [16]. The distances reported from MP2 optimisations for the central bonds were 1.87 and 1.793 Å for the outer ones [17].

A series of quite detailed studies of In_2O_3 systems were published recently. In 2010, Walsh and Woodley [18] reported the global minima for $(In_2O_3)_n$ clusters, n = 1–10, and for some additional higher-energy isomers. The authors employed an evolutionary algorithm technique at a first stage, followed by a refinement using the shell model [19] and subsequent DFT calculations. For the global minimum of the single molecule the authors found a 'flying gull'-type structure, in which the oxygen atoms at both ends are slightly bent down.

Mao-Jie *et al.* [20] studied different molecules of indium oxide, In_mO_n ($1 \le m, n \le 4$) at the DFT(B3LYP) level, using the 6-31G(d) basis set for oxygen atom and the effective core potential LanL2DZ for indium atom. For In_2O_3, their lowest-energy geometry is a rhombus-like structure with C_{2v} point symmetry, with total spin S = 1; the three In−O bond distances are 1.94, 1.95 and 1.99 Å. However, for the total spin $S = 0$, the most stable structure is linear, but the information concerning the bond distances and the electronic structure of the four studied isomers of In_2O_3 was not present.

In the study of Zhanpeisov *et al.* [21], the authors optimised the geometry of clusters $(In_2O_3)_n$ with n = 1–5 and 8. They inspected the geometry of several isomers of the clusters at the DFT (B3LYP) level with the LanL2DZ and SDD effective core potentials. For the monomer the linear ground state structure has two In−O single bonds of 1.902 Å in the centre of the molecule and two double bonds of 1.852 Å at both ends. The authors also mentioned that the linear structure was energetically favoured because it presented the oxidation number III for In atoms, while other isomers of the free In_2O_3 molecule had oxidation number II or IV.

The most recent study involving a single molecule of indium oxide was published by Panneerdoss *et al.* [22]; the reported geometry has V-shape. The molecular geometry was optimised while interacting with a bcc frame to simulate a layer of In_2O_3. The study also contains properties of thin film of indium oxide, determined through different experimental techniques. According to their CAM-B3LYP/3-21G(d,p) computations, the outer and the central bond distances are equal to 1.857 and 1.941 Å, respectively, and the central angle is around 129.4°. For the V geometry, they presented also the value of the dipole moment, d = 2.098 Debyes (0.825 ea_0) [22].

In the present paper, we analyse low-lying geometries of the In_2O_3 molecule and the molecule extracted from the crystal at the CCSD(T) level, which is the most precise computational method applied up to date to study In_2O_3. We calculated the dipole moments, electron affinity, ionisation potential and studied the nature of bonding. The crystal structure of In_2O_3 determined by Marezio [12] was used as the starting point for our study of the structure of In_2O_3 in the crystal. Using the crystallographic data we reproduced the coordination arrangement, in which each metallic centre was surrounded by six O atoms. From this arrangement the In_2O_3 geometry in crystal was extracted, see Subsection 3.1.

2. Methodology

In the ground state of the In_2O_3 molecule, the total spin $S = 0$. The calculations were performed at the coupled-cluster CCSD(T) [23–26] electron correlation level as implemented [27,28] in the 2010 version of MOLPRO suite of codes [29]. The scalar relativistic effects were taken into account by means of the Douglas–Kroll–Hess second-order scheme [30–32] with all-electron quadruple-ζ quality basis sets, QZP-DKH [33,34]. For the O atom the basis set is formed with (11s,7p,3d,2f,1g) Gaussian functions contracted to [6s,4p,3d,2f,1g] functions, thus comprising 58 spherical Gaussian functions [33]. For the In atom the basis set is constructed with (21s,17p,10d,3f,2g,1h) Gaussian functions, which are contracted to [10s,8p,5d,3f,2g,1h] functions that comprise 109 spherical Gaussian functions [34]. The number of configuration-state functions contained in the CCSD calculations is approximately 7.6×10^6. The respective basis sets were obtained from the Pacific Northwest National Laboratory database [35–37].

Although no restrictions were imposed by specifying a point group, we kept the centre of symmetry. For

the optimisations we used the quadratic steepest descent method [38] and these calculations were completed at the CCSD(T) level of theory, keeping tight convergence criteria: 10^{-6} for the gradient and 10^{-8} for the energy. Therefore, all reported energies are at the CCSD(T) level. The natural way for computing the dipole moment is to calculate it as the expectation value of the dipole operator. However, in MOLPRO the expectation values of one-electron operators can be computed with a precision not higher than the CCSD level of theory. Therefore, for the calculation of dipole moments at the CCSD(T) level we used the finite field method.

In order to determine the vertical ionisation potential (VIP) and the vertical electron affinity (VEA), the energies of the charged systems were computed by means of the restricted open-shell coupled cluster method, (RCCSD(T)) [23,39] as implemented in Molpro [40,41]. For obtaining the Natural Atomic populations, the transformation to Natural Atomic Orbitals (NAO) [42–44] was performed. The orbitals that were used in the transformation to NAO were the molecular natural orbitals obtained at the CCSD level, due to specifications of the suite of codes employed in MOLPRO. The program Avogadro [45] was our graphical interface to picture some results.

3. Results and discussion

In the following subsections, we will compare the properties of the In_2O_3 molecule extracted from the crystal and the optimised structures of the free indium oxide molecule. The results of our study of the dipole moments and some other properties of In_2O_3 will be also presented.

3.1. In_2O_3 extracted from crystal

In order to extract the structure of In_2O_3 from the crystal, we built the coordination arrangement obtained from a cubic C modification structure (bixbyite), according to the data reported by Marezio [12], see Figure 1. The arrangement corresponding to the cubic C modification was determined by Pauling and Shappell [46] for the mineral bixbyite, $(Fe, Mn)_2O_3$, following the studies of Zachariasen [47]. We chose the structure with most similar bond distances and nearly planar inside the coordination arrangement in the crystal lattice, where the In atoms are crystallographically non-equivalent. However, this feature was lost once the molecule has been extracted from a crystal cell. Nevertheless, the connexion with the specific environment of each type of In atom in the crystal structure is reflected in the different In-O bond distances that remained once the molecular structure has been extracted. Data of the bonds and angles of the molecule extracted from the crystal are collected in

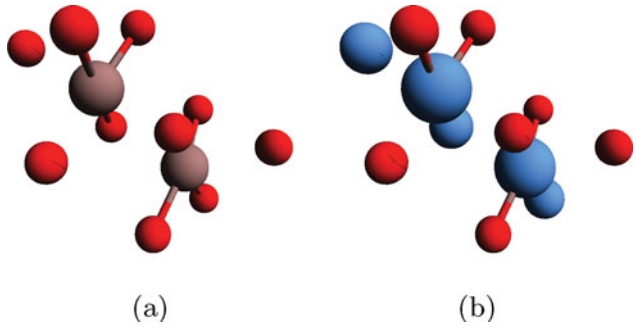

Figure 1. (a) The coordination arrangement [12], from which the molecule was extracted. (b) Atoms forming the molecular structure inside this arrangement depicted slightly bigger.

Table 1. Structural parameters of the In_2O_3 molecule extracted from the crystal.

Bond distance (Å)	Angles (deg.)	Dihedral (deg.)
$r_1 = 2.16$		
$r_2 = 2.16$	$\alpha_1 = 123.3$	
$r_3 = 2.18$	$\alpha_2 = 100.2$	$\theta_1 = -171.4$
$r_4 = 2.13$	$\alpha_3 = 100.8$	$\theta_2 = -166.7$

Table 1. In Table 1, the bond distances and the angles are labelled from left to right as r_1, r_2, r_3, r_4 and $\alpha_1, \alpha_2, \alpha_3$; the dihedral angles are θ_1 and θ_2. These parameters in Table 1 are organised as in the matrix of coordinates (Z-matrix). It is important to note that the zigzag structure that was extracted from the crystal is used as a type of reference to compare its properties with those of the free molecule. Certainly, this structure is optimum only in the crystal surrounding. Beyond the crystal it should not be stable.

The molecule extracted from the crystal has a zigzag structure and, besides being asymmetrical, it is not planar. It should be mentioned that in the coordination arrangement of the crystal the oxygen atoms are not exactly at the corners of a cube [12]. Even if we average of the interatomic distances from crystallographic data, the structure would not be symmetric because of the different angles. Due to the asymmetry of this zigzag-type structure, the 'crystal' molecule has a permanent dipole moment, see discussion in Subsection 3.3.

The comparative study of the molecular conformation extracted from the crystal and the free molecule conformations provides us with information about the changes in their geometries and some corresponding properties in the crystal field. It is also important to study a nanocluster extracted from the crystal and compare the results with the data obtained for an optimised nanocluster built of the free molecule. In this way, it may be possible to find properties observed in large systems that stem from the properties of free molecules or the molecules in the crystal field.

Table 2. The geometry and energy obtained at the CCSD(T) level for different conformations of the In_2O_3 molecule.

Structure	Outer bonds (Å)	Central bonds (Å)	In-O-In angle (deg.)	O-In-O angle (deg.)	Total energy (Hartree)[a]
V-shaped	1.842	1.933	144.3	180.0	–11 978.972 136 66
Linear	1.843	1.918	180.0	180.0	–11 978.971 353 80
DFT flying gull[b]	1.848	1.956	139.6	173.5	–11 978.970 864 73
From crystal[c]	-	-	-	-	–11 978.846 767 06

[a] Total energies of the optimised structures calculated at the CCSD(T)/QZP-DKH level and the energy of the molecule from crystal calculated at the same level.
[b] Calculated at the CCSD(T) level the 'flying-gull' DFT ground-state geometry found in Ref. [18].
[c] The structural parameters are taken from crystal and presented in Table 1.

3.2. Free In_2O_3 molecule

As we discuss in the previous subsection, for understanding the influence of the crystal field on the molecular geometry, it is instructive to study the free In_2O_3 molecule and compare its properties with the molecule extracted from the crystal. The optimisation of the free molecule structures was performed at the CCSD(T)/QZP-DKH level. The obtained results are presented in Table 2; the studied structures are depicted in Figure 2.

We based our optimisations on the reported structures of previous studies; namely: the linear, V-shaped geometry and the 'flying-gull' structure found by Walsh and Woodley [18] at the DFT level.

For the linear structure we optimised all bond distances. For the V-structure, the bond distances and the central angle (In-O-In) were optimised. In the DFT 'flying gull'- structure that has W-shape we optimised all four parameters: two bond distances, the central angle (In-O-In) and the angle corresponding to the 'wings' (O-In-O). It is important to note that the full optimisation at the CCSD(T) level of the 'flying gull'-type structure resulted in a V-type geometry with the same parameters that were found in independent optimisation of V-shaped structure.

According to Table 2, at the CCSD(T)/QZP-DKH level of theory the lowest energy is the V-shaped conformation. The linear conformation has the energy only on 0.02 eV (0.5 kcal/mol) higher. On the other hand, the energy of the 'flying-gull' DFT ground state geometry [18] calculated at the CCSD(T) level is on 0.01 eV higher than the linear one. All these energy differences are at the same order or smaller than the precision of our calculations. Therefore, although at the CCSD(T)/QZP-DKH level of theory the lowest is the V-shaped geometry, all three conformations in Table 2 can be possible candidates for the ground state of the In_2O_3 molecule.

As follows from Table 2, the bonds located at both ends of the two optimised structures are shorter than those in the middle. This tendency is in agreement with the findings of other studies [20–22]. The central bonds in the linear structure are slightly shorter than those in the V-shaped one. In the optimised geometries of the free molecule, all bond distances are shorter than those in the 'crystal' molecule, cf. with Table 1; this reflects the influence of interactions with the crystal surrounding. The energy of the molecule extracted from crystal is higher on 3.4 eV than the energy of the V-structure for free molecule. The reason for this is that the former structure is located inside the crystal field.

To the best of our knowledge, the CCSD(T)/QZP-DKH approach is the most precise calculation method applied at present for study the In_2O_3 molecule. We checked our results performing single-point calculations of optimised geometries at the CCSD(T) level with the larger atomic natural orbital-type basis set of Roos *et al.* [48]. The energetic order of molecular conformations in Table 2 remained the same, and the energy difference between the V-shape and linear structures increased only on 0.01 eV. However, it can be expected that the future application of more elaborated computational methods can increase the obtained energy differences or even will change the energetic order of the molecular conformations represented in Table 2.

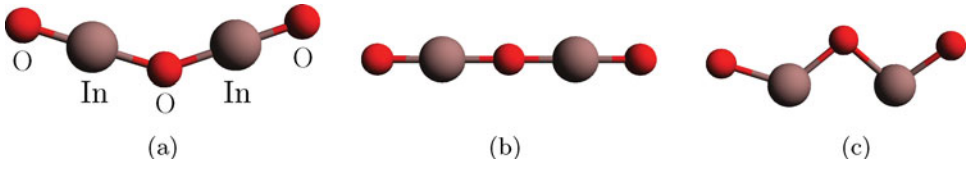

Figure 2. Conformations of the V-shaped (a), linear (b) and molecule extracted from the crystal (c).

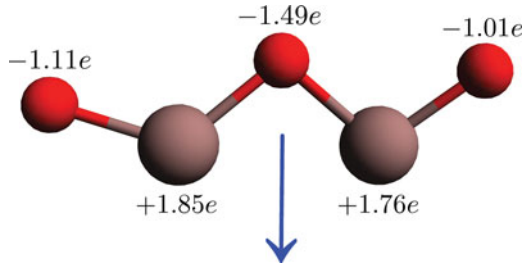

Figure 3. Charges on atoms in the molecule extracted from the crystal obtained from Natural Atomic population analysis. The arrow indicates the direction of the dipole moment.

3.3. Dipole moment

Besides the clear geometrical differences between the free molecule and the one extracted from the crystal, there are other physical differences. The molecule extracted from the crystal is not symmetric; it has a zigzag-type structure and possesses a permanent dipole moment. Its dipole moment computed at the CCSD(T) level is $d = 0.639\ ea_0$. In Figure 3 are shown the charges on atoms obtained from Natural Atomic population analysis (see Section 3.4) and the direction of the dipole moment in the In_2O_3 molecule extracted from the crystal .

The V-shaped structure, due to the bending angle, also has a dipole moment and its magnitude, at the CCSD(T) level, is $d = 0.773\ ea_0$. Thus, its value is slightly greater than the dipole moment of the molecule in the crystal (the linear structure, being symmetric, has no dipole moment). It is evident that a nanocluster extracted from the crystal can also possess *permanent* dipole moment. At the same time there is a mechanism to achieve essential value for the *induced* dipole moment. The dipole moment can arise on laser light absorption by a nanocluster. The principles of photoinduced diffusion transport of such nanoclusters in a polar environment, with laser pulse duration and duty cycle included as controllable variables, were analysed in Ref. [10]. A driving force of the photomotor considered is an external non-equilibrium periodic process of photoexcitation, which is generated by alternately switching on and off the laser radiation.

As an example, let us consider a cylindrical nanocluster with the height $h = 16$ Å and the radius $r = 7.5$ Å. In the absence of photoexcitation, there are no electrons located at a higher level than the valence band (if the solid state band model is at all applicable to such a small cluster). It is also likely that there are no donor impurities due to a small cluster size. This nanocluster can be ionised by excimer laser radiation. An electron thrown out from its bulk is then removed to the surface where it can be captured during diffusion by a trap on the surface, e.g., an oxygen vacancy. As far as nanocluster bulk ionisation followed by photoelectron surface trapping is concerned, the relevant energetic parameters should be taken into account. For $(In_2O_3)_n$ clusters, $n = 2$–10, ionisation potentials range from 7.1 to 8.1 eV (being close to the photon energies of conventional excimer lasers) and electron affinities range from 0.7 to 2.10 eV [18].

Table 3. The energies of the neutral and the charged In_2O_3 linear molecule computed at the CCSD(T) level and used for calculation of VIP and VEA.

Method	Energy (Hartree)
Neutral system	–11 978.971 353 80
Anion	–11 979.029 274 46[a]
Cation	–11 978.622 119 81[a]
Vertical ionisation potential	9.5 eV
Vertical electron affinity	1.6 eV

[a] The restricted open-shell approach, RCCSD(T).

For the free molecule VIP and VEA, as well as the total energies are represented in Table 3.

$VIP^{CCSD(T)} = 9.5$ eV and $VEA^{CCSD(T)} = 1.6$ eV. The VEA is in the range mentioned above for clusters; however, the VIP is larger than the value of 7.1 eV, reported by Klein *et al.* [49] from photoelectron spectroscopy measurement on thin films of In_2O_3. But it can be expected, since the value of IP on surface or in solid state is always decreased in comparison with the free molecule. In a similar way, it can be expected that the VIP of the cylindrical nanocluster may lie between the limits mentioned above.

The electron trapped on the surface and the hole in the bulk of the nanocluster form a dipole. The value of this photoinduced dipole moment is determined by the magnitude of the effective negative and positive charges and the distance between them. It can be roughly estimated as $d = 8\ ea_0$, a product of the electron charge and the cluster half-height, and appears to be rather large. On switching off the field, the induced dipole moment vanishes.

It is easy to see, the photoinduced dipole moment in a nanocluster arises differently from that induced by an electric field in a nonpolar molecule. Due to a tiny cluster size, the excitation of the second electron to the surface and, accordingly, the occurrence of another (possibly opposite) dipole are very improbable.

Since the interaction of a nanocluster with the polar periodic environment depends on its dipole moment, we can give rise to its directed motion by alternately switching on and off the laser or, in other words, by 'pushing' the nanocluster at the right time [8,9]. To this end, it is important that the laser pulse duration, duty cycle and laser-intensity dependent characteristic times of spontaneous and induced electronic transitions in the cluster correlate appropriately with the characteristic diffusion time over the potential period. These conditions were

Table 4. Natural Atomic populations of the valence shells in the In_2O_3 linear conformation.

Atom	Population of valence orbitals			Total	Charge
(1) O	$2s^{1.96}$	$2p^{5.49}$	$3d^{0.05}$	7.50	–1.50
(2) In	$5s^{0.40}$	$5p^{0.17}$	$5d^{0.0}$	0.57	+2.43
(3) O	$2s^{1.92}$	$2p^{5.88}$	$3d^{0.06}$	7.86	–1.86
(4) In	$5s^{0.40}$	$5p^{0.17}$	$5d^{0.0}$	0.57	+2.43
(5) O	$2s^{1.96}$	$2p^{5.49}$	$3d^{0.05}$	7.50	–1.50

Table 5. Natural Atomic populations of the valence shells in the In_2O_3 V-shaped conformation.

Atom	Population of valence orbitals			Total	Charge
(1) O	$2s^{1.96}$	$2p^{5.49}$	$3d^{0.05}$	7.50	–1.50
(2) In	$5s^{0.42}$	$5p^{0.17}$	$5d^{0.0}$	0.59	+2.41
(3) O	$2s^{1.93}$	$2p^{5.84}$	$3d^{0.05}$	7.82	–1.82
(4) In	$5s^{0.42}$	$5p^{0.17}$	$5d^{0.0}$	0.59	+2.41
(5) O	$2s^{1.96}$	$2p^{5.49}$	$3d^{0.05}$	7.503	–1.50

Table 6. Natural Atomic populations of the valence shells in In_2O_3 extracted from the crystal.

Atom	Population of valence orbitals			Total	Charge
(1) O	$2s^{1.99}$	$2p^{5.09}$	$3d^{0.03}$	7.11	–1.11
(2) In	$5s^{0.84}$	$5p^{0.31}$	$5d^{0.0}$	1.15	+1.85
(3) O	$2s^{1.97}$	$2p^{5.48}$	$3d^{0.04}$	7.49	–1.49
(4) In	$5s^{0.89}$	$5p^{0.35}$	$5d^{0.0}$	1.24	+1.76
(5) O	$2s^{1.97}$	$2p^{5.01}$	$3d^{0.03}$	7.01	–1.01

discussed in Ref. [10], where it was demonstrated that the In_2O_3 nanocluster with the above-mentioned parameters holds promise as a potential molecular photomotor.

3.4. The atomic population in the free and extracted from crystal In_2O_3 molecule and nature of bonding

To analyse the nature of bonding in the In_2O_3 molecule, we applied the Natural Atomic population analysis. The results for the free molecule are represented in Tables 4 and 5, for In_2O_3 extracted from the crystal are represented in Table 6. The electron population in the linear and V-structures is almost the same. Thus, the change in the central angle, at least in the range 180–140 degrees, practically has no effect on the population and does not change the bonds.

The central oxygen has negative charge of around −1.8 and the population of around 5.8*e* on the 2p orbitals, while the indium atoms are positively charged and have the population 0.17*e* on the 5p orbitals. Thus, the In atom has transferred most of the electron population of its 5p shell to the incomplete populated 2p orbitals of the central oxygen atom which leads to the formation of two single bonds with predominantly ionic character. Approximately 1.6*e* have been transferred from the 5 s orbitals to the oxygen atoms in the ends of the molecule, forming two double bonds. This leaves the In atoms with a positive charge +2.4, which is consistent with an oxidation number III.

From this analysis it follows that the chemical structure of the linear In_2O_3 can be represented as O = In−O−In = O, which agrees with the conclusion made by Zhanpeisov *et al.* [21]. The V-shaped molecule has the similar double- and single-bond structure. This means that the oxidation state of In atoms in these structures is in agreement with the reported oxidation state III of the metallic centres inside the crystal [50].

In Table 6, the results of Natural Atomic population analysis for In_2O_3 extracted from the crystal are represented. As follows from this table, the In atoms have the oxidation state II; this arises from the fact that the molecule extracted from the crystal is not in its original environment. The obtained charges on atoms allow us to find the direction of the dipole moment; these charges and the dipole moment are presented in Figure 3.

4. Conclusions

As follows from our results, see Table 2, the global minimum of optimised at the CCSD(T)/QZP-DKH level In_2O_3 corresponds to the V-shaped conformation. However, the energy difference among three presented geometries lies in the range of precision of our computational method. Hence, all three conformations can be considered as possible candidates for the ground state of the free In_2O_3 molecule at the CCSD(T)/QZP-DKH level. It should be mentioned that the method CCSD(T)/QZP-DKH applied in our study, to the best of our knowledge, is the most precise computational method used up to date to study the In_2O_3 molecule.

The geometry of the In_2O_3 molecule in crystal, which is obtained by extracting In_2O_3 from experimental crystal structure, was found essentially different from equilibrium geometries of the free In_2O_3 molecule. The geometry of In_2O_3 in crystal has a zigzag, completely asymmetric structure and possesses a dipole moment slightly smaller than the dipole moment of the V-structure of the free molecule. This reflects the influence of the crystal field on the molecular structure.

The molecules extracted from In_2O_3 crystal can be used as a 'bricks' for construction of different size nanoclusters. The action of electromagnetic radiation on these nanoclusters induces a comparatively large dipole moment that vanishes when the field is switched off. Therefore, as discussed in Subsection 3.3, this type of nanoclusters located in a polar environment can be used as a photomotor.

Acknowledgments

Authors acknowledge Alberto López Vivas for the computing facilities and technical support in programs used; U. Miranda wishes to express his gratitude to Consejo Nacional de Ciencia y Tecnología, México, for the postdoctoral grant 263485 to support this work.

Disclosure statement

No potential conflict of interest was reported by the authors.

Funding

State Program of RAS [project number 0082-2018-0003].

ORCID

Ulises Miranda http://orcid.org/0000-0002-2144-4191

References

[1] M. Chen, J. Xu, Y.-M. Liu, Y. Cao, H.-Y. He, and J.-H. Zhuang, Appl. Catal. A **377**, 35 (2010). doi:10.1016/j.apcata.2010.01.011.
[2] S. Santra, A. Majee, and A. Hajra, Tetrahedron Lett. **53**, 1974 (2012). doi:10.1016/j.tetlet.2012.02.021.
[3] S. Bahari and M.A. Sabegh, J. Chem. Sci. **125**, 153 (2013). doi:10.1007/s12039-012-0348-8.
[4] H. Yamaura, T. Jinkawa, J. Tamaki, K. Moriya, N. Miura, and N. Yamazoe, Sensor. Actuat. B **35–36**, 325 (1996). doi:10.1016/S0925-4005(97)80090-1.
[5] W.-Y. Chung, G. Sakai, K. Shimanoe, N. Miura, D.-D. Lee, and N. Yamazoe, Sensor. Actuat. B **46**, 139 (1998). doi:10.1016/S0925-4005(98)00100-2.
[6] L.I. Trakhtenberg, G.N. Gerasimov, V.F. Gromov, T.V. Belysheva, and O.J. Ilegbusi, Sensor. Actuat. B **169**, 32 (2012). doi:10.1016/j.snb.2012.01.064.
[7] L.I. Trakhtenberg, G.N. Gerasimov, V.F. Gromov, T.V. Belysheva, and O.J. Ilegbusi, Sensor. Actuat. B **187**, 514 (2013). doi:10.1016/j.snb.2013.03.017.
[8] S. Saha and J.F. Stoddart, Chem. Soc. Rev. **36**, 77 (2007). doi:10.1039/B607187B.
[9] P. Hänggi and F. Marchesoni, Rev. Mod. Phys. **81**, 387 (2009). doi:10.1103/RevModPhys.81.387.
[10] V.M. Rozenbaum, M.L. Dekhtyar, S.H. Lin, and L.I. Trakhtenberg, J. Chem. Phys. **145**, 064110 (2016). doi:10.1063/1.4960622.
[11] J.P. Remeika and E.G. Spencer, J. Appl. Phys. **35**, 2803 (1964). doi:10.1063/1.1713110.
[12] M. Marezio, Acta Cryst. **20**, 623 (1966). doi:10.1107/S0365110X66001749.
[13] C.I. Bright, in *50 Years of Vacuum Coating Technology and Growth of the Society of Vacuum Coaters*, edited by D.M. Matox and V.H. Matox (SVC, Albuquerque, New Mexico, United States, 2007), pp. 38–45.
[14] A. Walsh, J.L.F. da Silva, S.-H. Wei, C. Körber, A. Klein, L.F.J. Piper, A. DeMasi, K.E. Smith, G. Panaccione, P. Torelli, D.J. Payne, A. Bourlange, and R.G. Edgell, Phys. Rev. Lett. **100**, 167402 (2008). doi:10.1103/PhysRevLett.100.167402.
[15] J. Robertson and B. Falabretti, in *Handbook of Transparent Conductors*, edited by D.S. Ginley (Springer, New York, United States, 2011) pp. 27–50.
[16] T.R. Burkholder, J.T. Yutsein, and L. Andrews, J. Phys. Chem. **96**, 10189 (1992). doi:10.1021/j100204a019.
[17] E.F. Archibong and R. Sullivan, J. Phys. Chem. **100**, 18078 (1996). doi:10.1021/jp961571+.
[18] A. Walsh and S.M. Woodley, Phys. Chem. Chem. Phys. **12**, 8446 (2010). doi:10.1039/c0cp00056f.
[19] B.G. Dick and A.W. Overhauser, Phys. Rev. **112**, 90 (1958). doi:10.1103/PhysRev.112.90.
[20] X. Mao-Jie, N. Yi, L. Zhen-Qing, W. Sheng-Li, L. Xiao-Hui, and D. Xiao-Ming, Chin. Phys. B **20**, 063101 (2011). doi:10.1088/1674-1056/20/6/063101.
[21] N.U. Zhanpeisov, H. Nakatani, and H. Fukumura, Res. Chem. Intermed. **37**, 647 (2011). doi:10.1007/s11164-011-0239-5.
[22] I.J. Panneerdoss, S.J. Jeyakumar, S. Ramalingam, and M. Jothibas, Spectrochim. Acta A **147**, 1 (2015). doi:10.1016/j.saa.2015.02.033.
[23] M. Rittby and R.J. Bartlett, J. Phys. Chem. **92**, 3033 (1988). doi:10.1021/j100322a004.
[24] R. J. Bartlett, J. D. Watts, S. A. Kucharski, and J. Noga, Chem. Phys. Lett. **165**, 513 (1990); **167**, 609 (1990). doi:10.1016/0009-2614(90)87031-L.
[25] M. Urban, J. Noga, S.J. Cole, and R.J. Bartlett, J. Chem. Phys. **83**, 4041 (1985). doi:10.1063/1.449067.
[26] K. Raghavachari, G.W. Trucks, J.A. Pople, and M. Head-Gordon, Chem. Phys. Lett. **157**, 479 (1989). doi:10.1016/S0009-2614(89)87395-6.
[27] C. Hampel, K. Peterson, and H.-J. Werner, Chem. Phys. Lett. **190**, 1 (1992). doi:10.1016/0009-2614(92)86093-W.
[28] M.J.O. Deegan and P.J. Knowles, Chem. Phys. Lett. **227**, 321 (1994). doi:10.1016/0009-2614(94)00815-9.
[29] H.-J. Werner, P.J. Knowles, G. Knizia, F.R. Manby, M. Schütz, P. Celani, T. Korona, R. Lindh, A. Mitrushenkov, G. Rauhut, K.R. Shamasundar, T.B. Adler, R.D. Amos, A. Bernhardsson, A. Berning, D.L. Cooper, M.J.O. Deegan, A.J. Dobbyn, F. Eckert, E. Goll, C. Hampel, A. Hesselmann, G. Hetzer, T. Hrenar, G. Jansen, C. Köppl, Y. Liu, A.W. Lloyd, R.A. Mata, A.J. May, S.J. McNicholas, W. Meyer, M.E. Mura, A. Nicklass, D.P. O'Neill, P. Palmieri, K. Pflüger, R. Pitzer, M. Reiher, T. Shiozaki, H. Stoll, A.J. Stone, R. Tarroni, T. Thorsteinsson, M. Wang, A. Wolf, Molpro, version 2010.1, a package of ab initio programs, 2010. <http://www.molpro.net>.
[30] M. Douglas and N.M. Kroll, Ann. Phys. (N.Y.) **82**, 89 (1974). doi:10.1016/0003-4916(74)90333-9.
[31] B.A. Hess, Phys. Rev. A **32**, 756 (1985). doi:10.1103/ PhysRevA.32.756.
[32] B.A. Hess, Phys. Rev. A **33**, 3742 (1986). doi:10.1103/ PhysRevA.33.3742.
[33] F.E. Jorge, A. Canal Neto, G.G. Camiletti, and S.F. Machado, J. Chem. Phys. **130**, 064108 (2009). doi:10.1063/1.3072360.
[34] G.A. Ceolin, R.C. de Berrêdo, and F.E. Jorge, Theor. Chem. Acc. **132**, 1339 (2013). doi:10.1007/s00214-013-1339-7.
[35] Basis set exchange. <https://bse.pnl.gov/bse/portal>.

[36] D. Feller, J. Comp. Chem. **17**, 1571 (1996). doi:10.1002/(SICI)1096-987X(199610)17:13%3c1571::AID-JCC9%3e3.0.CO;2-P.
[37] K.L. Schuchardt, B.T. Didier, T. Elsethagen, L. Sun, V. Gurumoorthi, J. Chase, J. Li, and T.L. Windus, J. Chem. Inf. Model. **47**, 1045 (2007). doi:10.1021/ci600510j.
[38] J. Sun and K. Ruedenberg, J. Chem. Phys. **99**, 5257 (1993). doi:10.1063/1.465994.
[39] J.D. Watts, J. Gauss, and R.J. Bartlett, J. Chem. Phys. **98**, 8718 (1993). doi:10.1063/1.464480.
[40] P.J. Knowles, C. Hampel, and H.-J. Werner, J. Chem. Phys. **99**, 5219 (1993). doi:10.1063/1.465990.
[41] P.J. Knowles, C. Hampel, and H.-J. Werner, J. Chem. Phys. **112**, 3106–3107 (1993). doi:10.1063/1.480886.
[42] A.E. Reed and F. Weinhold, J. Chem. Phys. **78**, 4066 (1983). doi:10.1063/1.445134.
[43] A.E. Reed, R.B. Weinstock, and F. Weinhold, J. Chem. Phys. **83**, 735 (1985). doi:10.1063/1.449486.
[44] A.E. Reed and F. Weinhold, J. Chem. Phys. **83**, 1736 (1985). doi:10.1063/1.449360.
[45] M.D. Hanwell, D.E. Curtis, D.G. Lonie, T. Vandermeersch, E. Zurek, and G.R. Hutchison, J. Cheminformatics **4**, 17 (2012). doi:10.1186/1758-2946-4-17.
[46] L. Pauling and M.D. Shappell, Z. Krist. **75**, 128 (1930).
[47] W.H. Zachariasen, Z. Krist. **67**, 455 (1928).
[48] B.O. Roos, R. Lindh, P.-A. Malmqvist, V. Veryazov, and P.-O. Widmark, J. Phys. Chem. A **108**, 2851 (2004). doi:10.1021/jp031064+.
[49] A. Klein, C. Körber, A. Wachau, F. Säuberlich, Y. Gassenbauer, R. Schafranek, S.P. Harvey, and T.O. Mason, Thin Solid Films **518**, 1197 (2009). doi:10.1016/j.tsf.2009.05.057.
[50] A.F. Holleman, E. Wiberg, N. Wiberg, and G. Fischer, *Lehrbuch der anorganischen Chemie* (Walter de Gruyter, Berlin, 2007), pp. 1185–1186.